Effect of Morphology and Pore Size of Sulfonated Mesoporous Benzene-silicas in the Preparation of Poly(vinyl alcohol)-Based Hybrid Nanocomposite Membranes for Direct Methanol Fuel Cell Application

Eun-Bum Cho, Hoyoung Kim, and Dukjoon Kim*

Department of Chemical Engineering, Polymer Technology Institute, Sungkyunkwan University, Suwon, Gyeonggi-do 440-746, Korea

Received: January 22, 2009; Revised Manuscript Received: June 7, 2009

Sulfonated mesoporous benzene-silicas were introduced into a poly(vinyl alcohol) (PVA) polymer matrix to act as a barrier for methanol crossover, to prepare composite electrolyte membranes for direct methanol fuel cell applications. Highly ordered 2D hexagonal mesoporous benzene-silicas were prepared using 1,4-bis(triethoxysilyl)benzene (BTEB) organosilica precursor and two kinds of organic templates, such as an octadecyltrimethylammonium bromide (ODTMA) and a Pluronic P123 poly(ethylene oxide)−poly(propylene oxide)−poly(ethylene oxide) (PEO−PPO−PEO) triblock copolymer, to investigate the effect of the morphology and the pore size on the methanol permeability and the proton conductivity of the membranes. The sulfonated mesoporous benzene-silica and PVA were mixed with a sulfosuccinic acid (SSA) cross-linker to improve the membrane stability from mechanical and conductive viewpoints. The physical and chemical characterization of the hybrid electrolyte membranes was performed by varying the contents of sulfonated mesoporous benzene-silicas and SSA. All the hybrid membranes studied showed good performance in lowering the methanol crossover (i.e., ∼68% reduction in comparison with the Nafion117 membrane), and mesoporous benzene-silica with smaller particle morphology and pores (2−3 nm) was observed to be a more effective additive.

Introduction

Direct methanol fuel cells (DMFC) using methanol fuel with a high energy density are known as an attractive potential replacement for secondary lithium-ion batteries in portable devices.[1−3] Although a lot of new technology has been developed for DMFC operation, the energy conversion efficiency of DMFCs is still low, which is attributed primarily to the methanol crossover from the anode to the cathode caused by electro-osmotic drag.[4−6] Recent works have also suggested that the reactive free radicals formed at the cathode due to the methanol crossover may lead to the catastrophic failure of the polymer electrolyte membranes.[7−10] Therefore, one of the major targets in the development of proton conductive electrolyte membranes is to reduce the fuel crossover while maintaining a high proton conductivity.[6,11−13] Although Nafion, the most widely used perfluorosulfonic acid-based polymer membrane, possesses good properties such as high proton conductivity, processability, and high mechanical and chemical stability, it still has a couple of major drawbacks associated with its high methanol crossover and high cost. The development of fluorine-free membranes has been one of the research directions which is attemptimg to reduce the economic problem. There have been two main approaches to the improvement of the membrane performance: one is to synthesize new types of polymers and the other is to modify the existing polymer membranes by incorporating a methanol barrier. Hydrocarbon-based polymers such as sulfonated polystyrene and its copolymers and sulfonated aromatic polymers such as sulfonated poly(aryrene ether), poly(ether ether ketone), and polyimide have been studied.[14−20] The latter approach is to incorporate various inorganic fillers, which are known to alter the transport properties as well as mechanical stability of the membranes.[21−29] Various functionalized silica and organosilica precursors have been investigated, and moreover, recently, porous materials such as zeolite and functionalized mesoporous silica materials have been used to prepare more efficient electrolyte membranes.[23,26] In the preparation of hybrid membranes containing more than two components, the compatibility between the components is a crucial factor, and a considerable amount of research has been conducted on their modification.

Commercial poly(vinyl alcohol) (PVA), which exhibits a preference for water molecules compared to methanol or ethanol, has been widely used to prepare specific films, adhesives, and membranes. PVA membranes themselves have been reported to be better methanol barriers than Nafion membranes due to their dense molecular packing structure caused by inter- and intramolecular hydrogen bonding. On the other hand, there are no negatively charged ions in the PVA chains to transport protons.[30,31] Recently, the potential use of various sulfonated PVA membranes with additives in DMFC membranes has been investigated.[32−40]

Mesoporous silica materials have been developed extensively for various applications due to their high surface area, narrow pore size distribution, and adjustable mesopore size.[41−45] The morphology and texture as well as the porosity can alter optical, electronic, mechanical, and catalytic behavior of materials. The surface hydrophobic/hydrophilic and reactive properties of mesoporous materials were also tuned by the attachment of various organic moieties. The development of periodic mesoporous organo-silicas (PMOs) opened up new possibilities for the synthesis of particles with desired properties.[46−50] Mesoporous channels, even if they are not arranged in the uniform anisotropic form, can be used as conductive tunnels of protons

* Corresponding author. Phone: +82-31-290 7250. E-mail: djkim@skku.edu.

10.1021/jp9006763 CCC: $40.75
Published on Web 07/01/2009

and water molecules and so on. This report is concerned with the use of mesoporous organo-silica materials to reduce the methanol crossover while maintaining the other properties.

Herein, we report the preparation and characterization of a PVA-based hybrid electrolyte membrane using sulfonated mesoporous benzene-silicas and sulfosuccinic acid as additives. First, we prepared mesoporous benzene-silica using an octadecyltrimethylammonium bromide (ODTMA) cationic surfactant and a Pluronic P123 poly(ethylene oxide)−poly(propylene oxide)−poly(ethylene oxide) (PEO−PPO−PEO) nonionic triblock copolymer as structure-directing agents and 1,4-bis(triethoxysilyl)benzene (BTEB) as an organosilica precursor. The benzene-bridged silsesquioxane that is used has both hydrophobic and hydrophilic properties, and the additive sulfonic acids can be attached to the benzene-bridging groups by the post-treatment step. The benzene moieties are expected to increase the thermal and mechanical stability, which is the weak point of the poly(vinyl alcohol) matrix. Above all, mesoporous materials have the advantage of retaining waters even at a high temperature, due to the capillary force of the mesopores, and the large number of pores arranged in hexagonal patterns can be used as tunnels to transport protons. The pore size and the morphology of mesoporous materials are altered by the templates that are used; the ODTMA-driven mesoporous benzene-silica has a pore diameter of 2−3 nm and shows mixed morphologies composed of agglomerates of spherical particles with a particle size below 100 nm and thin rods with a thickness on the nanometer scale. On the other hand, the P123-driven material has mesopores with a pore diameter of 6−7 nm and shows a cylindrical rod-type morphology and its bundles; however, their thickness and length scales are not uniform in the range of 1−100 μm. PVA and mesoporous benzene-silica are mixed with each other by using a cross-linking agent containing a sulfonic acid group, i.e., sulfosuccinic acid (SSA). SSA containing reactive carboxylic acid groups is also used to reduce the channel size of the PVA chains by the esterification reaction with the hydroxyl groups in PVA. The SSA molecules in this three-component mixture studied herein would be expected to lead to partial chemical linkages between the PVA and mesoporous materials, as well as to retain the proton conductivity. This attempt at preparing a PVA/mesoporous material hybrid nanocomposite electrolyte membrane was made to examine the effect of mesoporous organo-silica materials on the transport properties of protons and methanol, and this report is focused on the effect of the morphology and the pore size of the sulfonated mesoporous benzene-silicas inside the hybrid membrane using the aforementioned two kinds of mesoporous materials. In this report, a detailed analysis of the PVA-based hybrid nanocomposite membranes composed of well-defined mesoporous benzene-silicas and a reactive SSA cross-linker is presented from the chemical and structural points of view. The relationship between the structure and transport properties is also discussed.

Experimental Section

Materials. Poly(vinyl alcohol) (PVA, average M_w: 124 000−186 000, 99+% hydrolyzed) (Aldrich) was used as a polymer matrix, and sulfosuccinic acid (SSA, 70 wt % solution in water) (Aldrich) was used as a cross-linker. Octadecyltrimethylammonium bromide (ODTMA) (Aldrich) and Pluronic P123 triblock copolymer ($EO_{20}PO_{70}EO_{20}$) (BASF) were used as soft templates to prepare the 2D hexagonal mesostructures. 1,4-Bis(triethoxysilyl)benzene (BTEB) (Aldrich) was used as a bridged organosilica precursor. Sulfuric acids (30% SO_3/H_2SO_4 fuming agent and 95−98% H_2SO_4) (Aldrich), hydrochloric acid solution (37 wt %) (Aldrich), and methanol (Aldrich) were all analytical-grade reagents and used without further purification. Distilled water was also used to prepare the PVA composite membranes.

TABLE 1: Nomenclature and the Corresponding Weights in the Preparation of PVA/SSA/Mesoporous Benzene-silica Hybrid Membranes

sample	PVA (wt %)	SSA (wt %)	sOBS (wt %)	sample	PVA (wt %)	SSA (wt %)	sPBS (wt %)
OBS210	88	2	10	PBS210	88	2	10
OBS220	78	2	20	PBS220	78	2	20
OBS230	68	2	30	PBS230	68	2	30
OBS510	85	5	10	PBS510	85	5	10
OBS520	75	5	20	PBS520	75	5	20
OBS530	65	5	30	PBS530	65	5	30
OBS710	83	7	10	PBS710	83	7	10
OBS720	73	7	20	PBS720	73	7	20
OBS730	63	7	30	PBS730	63	7	30

Preparation of Periodic Mesoporous Benzene-silica. In a typical synthesis of a PMO sample using ODTMA surfactant, 3.76 g of ODTMA was dissolved in an NaOH solution, a mixture of 100.0 g of distilled water and 8.0 g of 6 M NaOH, under vigorous stirring at 60 °C. Then, 4.0 g of the BTEB organosilica precursor was added, and the stirring was continued for about 20 h at 25 °C. In the case of the PMO sample using a P123 block copolymer, 3.92 g of the P123 triblock copolymer was dissolved in a mixture of 142.6 g of distilled water and 0.79 g of HCl (37 wt %, Aldrich) under vigorous stirring. Next, 4.0 g of the BTEB organosilica precursor was added, and the stirring was continued for about 12 h at 40 °C, which resulted in the formation of a white precipitate. The solid products were aged for 24 h at 100 °C. The surfactant and block copolymer template in the obtained solids were extracted by successive treatment with an adequate quantity of ethanol for 2 h under a static condition and 120 mL of acetone at 56 °C under stirring for 10 h, followed by washing with distilled water and acetone using a suction flask and drying at 100 °C for 1 day.

Sulfonation of Periodic Mesoporous Benzene-silicas. An amount of 2 g of ODTMA-driven mesoporous benzene-silica powder (OBS) was mixed with 500 mL of fuming agent (30% SO_3/H_2SO_4) and placed in an oil bath for 10 h at 105 °C under static condition. The dispersion was cooled to room temperature and added to 2000 mL of distilled water. The sulfonated solid was washed and filtered with boiling water, ethanol, and acetone solvents repeatedly using a suction flask. Then, the solid was protonated by stirring it in 500 mL of 6 M hydrochloric acid aqueous solution for 24 h, followed by washing and filtering with distilled water and acetone. In the case of the P123-driven mesoporous powder (PBS), 2 g of the solid was mixed with 500 mL of sulfuric acid (98%) and stirred for 2 days at room temperature. The mixed solution was cooled at room temperature and added to 2000 mL of distilled water. Then, the mesoporous solid was washed, filtered, and protonated by the aforementioned method. In the case of the sulfonation of the PBS powders, no fuming agent was used due to the low yield of the final precipitates.

Preparation of PVA/Mesoporous Benzene-silica Hybrid Membrane. An amount of 150 g of 6 wt % PVA aqueous solution was prepared by dissolving 9 g of PVA powder in 141 g of distilled water with stirring for 6 h at 90 °C and for 12 h at room temperature. The two kinds of sulfonated mesoporous benzene-silicas (denoted as "sOBS" and "sPBS") and SSA were added to 15 g of PVA solution based on the corresponding weight ratios, as shown in Table 1. Then, the mixed PVA

solutions were stirred for 4 h at 45 °C and sonicated for 30 min at room temperature. After stirring the solutions for 10 min more at 45 °C, composite membranes were prepared by pouring the solutions onto a stainless steel plate, followed by casting them using the doctor blade process. The cast solutions were dried for 1 day in air at room temperature and cross-linked in an oven for 1 h at 120 °C. The final cross-linked hybrid membranes were peeled from the plate and kept in vials containing an adequate quantity of distilled water and in a vacuum separately. The sample names for the final composite membranes are listed in Table 1.

Characterization of Mesoporous Materials and Nanocomposite Membranes. ***X-ray Scattering.*** The small-angle X-ray scattering experiments were performed using a Bruker SAXS analyzer having a 2D GADDS diffractometer and Cu Kα radiation with $\lambda = 1.54$ Å. Synchrotron SAXS was also performed using $\lambda = 1.608$ Å radiation at PAL in POSTECH. The wide-angle X-ray measurements were performed using a Bruker WAXS analyzer with a 600 mm goniometer and a 2D area detector. The 2D WAXS data were collected and converted to spectra versus 2θ values in the range from 5 to 40 degrees.

Transmission and Scanning Electron Microscopy. The TEM images were obtained with an FE-TEM (JEOL JEM2100F) operated at an accelerating voltage of 200 kV. The mesoporous samples were sonicated for 60 min in an adequate quantity of acetone, and the solution was dropped onto a porous carbon film on a copper grid and then dried in a vacuum. For the composite membranes, the samples were prepared by cutting them into slices using a microtome after molding them with epoxy. SEM conjunction with energy dispersive X-ray spectroscopy (EDS) was performed with a field emission SEM (Philips XL30 ESEM-FEG) operating at an accelerating voltage of 30 kV.

Nitrogen Adsorption Isotherm. The nitrogen adsorption−desorption isotherms were measured on a Micromeritics 2010 analyzer. The sulfonated benzene-silica mesoporous samples were degassed at 150 °C to achieve a vacuum of less than 30 μmHg. The BET (Brunauer−Emmet−Teller) specific surface area was calculated from the adsorption data in the relative pressure range from 0.05 to 0.2. The total pore volume was evaluated from the amount of gas adsorbed at a relative pressure of 0.99. The PSD curves were calculated from the adsorption branches of the isotherms using the BJH method. The pore width was estimated from the maximum of the PSD curve.

Infrared Spectroscopy. An attenuated total reflection Fourier transform infrared spectrometer (ATR-FTIR, Bruker IFS-66/S, Bruker) was used to identify the chemical structure, the cross-linking, the sulfonation reaction, and the chemical linkage between the mesoporous benzene-silica additives and the PVA polymer matrix of the composite membrane.

Ion-Exchange Capacity. The ion-exchange capacities (IECs) of the sulfonated benzene-silica mesoporous samples were determined by a titration method using a 2 M aqueous solution of sodium chloride. In a typical experiment, 0.05 g of the solid was added to 10 mL of NaCl aqueous solution and stirred for 24 h. The resulting suspension was allowed to equilibrate and titrated potentiometrically by the dropwise addition of a 0.01 N NaOH solution using a pH meter (Orion 420A). IECs of the sulfonated benzene-PMOs were also determined through the evaluation of sulfur atom using an elemental analyzer (Flash EA 1112, Thermo Electron). The IECs of the PVA membranes were determined by a titration method similar to that used for the benzene-silica powders. For the composite membranes, 0.1 g of membrane, 10 mL of NaCl, and 0.01 N of NaOH were used in the respective steps of the aforementioned experimental procedure.

Water Uptake. The water uptake of the composite membranes was measured at room temperature by a gravitational method. All of the membranes were kept in vacuum desiccators containing P_2O_5 for a week. After the dry membranes were weighed, the samples were placed in distilled water, during which time the sample was periodically weighed until no further weight gain was detected. The water uptake of the membrane was determined from eq 1

$$\text{water uptake } (\%) = (W_{\text{wet}} - W_{\text{dry}}) \times 100/W_{\text{dry}} \quad (1)$$

Here, W_{wet} and W_{dry} indicate the weights of wet membrane at equilibrium and dry membrane, respectively.

Thermal Properties. A thermogravimetric analyzer (TGA, TGA7, Perkin-Elmer) was used to analyze the thermal stability of the composite membranes. The weight of the samples was scanned from 25 to 800 °C at a ramping rate of 10 °C/min under a nitrogen flow.

Methanol Permeability. The methanol permeability was measured at room temperature using a glass diffusion cell where the membrane was located in the middle. The left compartment was filled with 50 mL of 2 M methanol aqueous solution, and the right one with 50 mL of distilled water. Magnetic stirring was employed in each compartment to ensure the uniform distribution of methanol. The methanol concentration in the water compartment was measured in situ by an RI detector (RI750F, Younglin). The methanol permeability (P) was calculated from eq 2

$$C_{\text{B}}(t) = (A/V_{\text{B}})(P/L)C_{\text{A}}(t - t_0) \quad (2)$$

Here, C_{A} and C_{B} are the methanol concentrations in the left (MeOH) and the right (water) compartments, respectively. A is the membrane surface area; L is the membrane thickness; and V_{B} is the volume of the right compartment.

Proton Conductivity. 2-Probe impedance spectroscopy (Solartron 1260, Solartron) was used to determine the ion conductivity of the composite membranes. The resistance (impedance) was measured in the frequency range of 10^2-10^6 Hz under the applied load potential of 10 mV and the relative humidity of 90% at room temperature. The proton conductivity (Ã) was calculated from eq 3

$$\text{proton conductivity } \tilde{\text{A}}(\sigma, \text{S/cm}) = L(\text{cm})/[R(\Omega) \times A(\text{cm}^2)] \quad (3)$$

Here, L is the distance between the electrodes used to measure the potential; R is the impedance of the membrane; and A is the surface area of the membrane.

Results and Discussion

Characterization of Sulfonated Meoporous Benzene-silica. Two kinds of sulfonated benzene-silica (sOBS and sPBS) powders were synthesized in the presence of an ODTMA cationic surfactant and a Pluronic P123 nonionic block copolymer as described in the experimental section. The small-angle X-ray scattering patterns for these two kinds of sulfonated benzene-silica powders are shown in the left panels (a-1, b-1) of Figure 1. As can be seen from Figure 1 (a-1, b-1), the

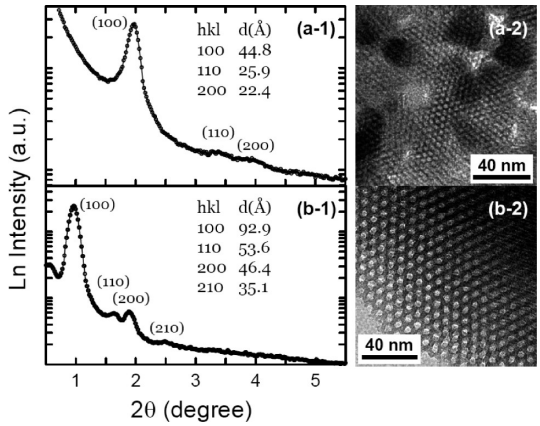

Figure 1. SAXS patterns and TEM images for two kinds of sulfonated mesoporous benzene-silicas: (a-1) and (a-2) are for ODTMA-driven mesoporous benzene-silica (sOBS), and (b-1) and (b-2) are for P123-driven benzene-silica (sPBS) powder, respectively.

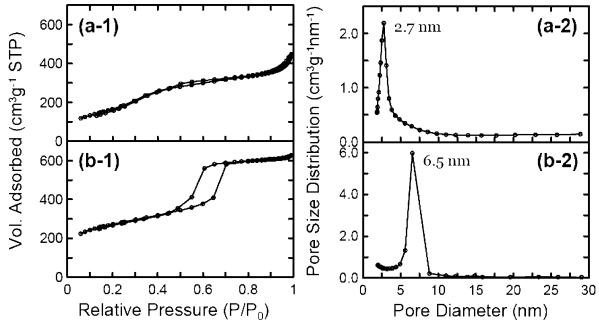

Figure 2. Nitrogen adsorption−desorption isotherms and pore size distributions for sulfonated mesoporous benzene-silicas: (a-1) and (a-2) are for ODTMA-driven mesoporous benzene-silica (sOBS), and (b-1) and (b-2) are for P123-driven benzene-silica (sPBS) powder, respectively.

sulfonated benzene-silicas exhibit highly ordered 2D hexagonal (*p6mm*) mesophases with three and four well-resolved peaks indexed as (100), (110), (200), and (210) reflections. The most intense (100) peaks represent the *d*-spacing values of 4.48 and 9.29 nm, which correspond to the unit cell parameters (*a*) of 5.17 and 10.73 nm, respectively. The TEM images shown in the right panels (a-2, b-2) of Figure 1 also clearly demonstrate the presence of well-defined 2D hexagonal (*p6mm*) mesostructures, and the size difference is consistent with the characteristic sizes estimated by SAXS analysis.

The nitrogen adsorption−desorption isotherms for the sulfonated benzene-silicas are shown in Figure 2. The isotherm for sOBS without any hysteresis is the typical pattern of a mesoporous silica prepared with a cationic surfactant,[50] while that for sPBS is type IV with a steep increase of the adsorption branch at $P/P_0 = 0.65-0.75$ due to the capillary condensation of nitrogen, which is a characteristic feature of mesoporous silica-based materials templated with block copolymers, as shown in Figure 2(b-1). The BET surface areas of sOBS and sPBS samples are obtained as 613 and 964 m^2g^{-1}, respectively. The total pore volumes are 0.68 and 0.97 cm^3g^{-1}, respectively, and the pore size distributions (PSD) obtained from the adsorption branch of the isotherms by the BJH method are narrow, indicating the high uniformity of the porous structures, as shown in Figure 2(a-2, b-2). The pore diameters determined at the maximum of the PSDs are 2.7 and 6.5 nm for sOBS and sPBS samples, respectively. The wall thicknesses show increased values of 2.5 and 4.2 nm, respectively, due to the sulfonation of the benzene-bridging group and the protonation. The ion

TABLE 2: Physicochemical Properties of Sulfonated Benzene-silica Powders Prepared with Two Kinds of Templates[a]

sample	template	S_{BET} (m^2 g^{-1})	V_t (cm^3 g^{-1})	a (nm)	D_p (nm)	W (nm)	IEC (meq/g)
sOBS	ODTMA	613	0.68	5.17	2.7	2.5	0.60,[b] 0.56[c]
sPBS	P123	964	0.97	10.73	6.5	4.2	0.08,[b] 0.05[c]

[a] sOBS, sulfonated benzene-silica prepared with an ODTMA surfactant; sPBS, sulfonated benzene-silica prepared with a P123 block copolymer; S_{BET}, BET specific surface area; V_t, total pore volume; a, unit cell parameter ($= d_{100} \times 2/\sqrt{3}$); D_p, mesopore diameter determined at the maximum of pore size distributions (PSDs) calculated by the BJH method; W, pore wall thickness ($= a - D_p$). [b] IEC, ion exchange capacity obtained by titration. [c] Elemental analysis, respectively (= sulfonation degree).

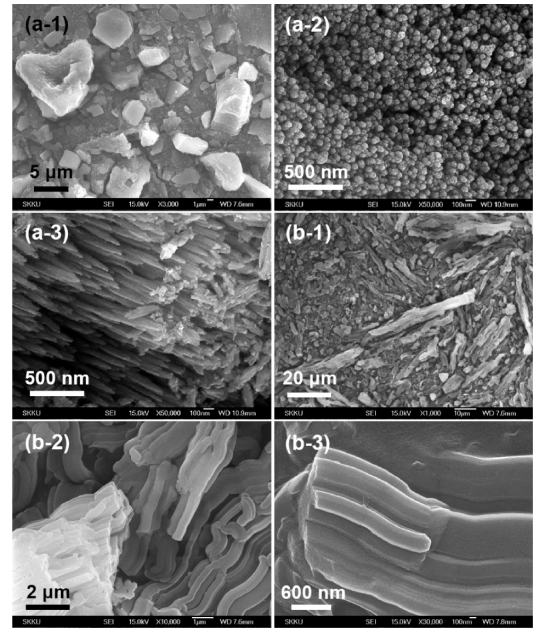

Figure 3. SEM images for sulfonated mesoporous benzene-silicas: (a-1), (a-2), and (a-3) are for ODTMA-driven mesoporous benzene-silica (sOBS) powder, and (b-1), (b-2), and (b-3) are for P123-driven benzene-silica (sPBS), respectively.

exchange capacities for sOBS and sPBS solid powders were determined to be 0.60 and 0.08 meq/g solid by the titration method, respectively, which indicates that the benzene moieties of the sPBS sample buried in the thicker wall are harder to modify with sulfonic acids. The overall physicochemical properties are summarized in Table 2.

The morphologies for the sOBS and sPBS samples are shown in Figure 3. Figure 3(a-1, a-2, and a-3) present the FE-SEM images at different magnification levels for the sOBS powders, and Figure 3(b-1, b-2, and b-3) present those for the sPBS powders. The sOBS powders show irregular particles with a diameter of 1−10 μm at low magnification (Figure 3(a-1)); however, the enlarged fragments of the images reveal that the irregular particles consist of agglomerates of uniform spherical nanoparticles having a particle diameter of less than 100 nm and thin cylindrical rods with a thickness on the nanometer scale, as shown in Figure 3(a-2, a-3). On the other hand, the sPBS solid powders show bundles of cylindrical rods with thicknesses and lengths in the range of 1−100 μm at both the low and high magnification levels in Figure 3(b-1, b-2, and b-3), and the sizes of the cylindrical rods are thicker and longer than those of the sOBS particles as can be seen in Figure 3. The SEM images demonstrate that the morphology of the mesoporous benzene-

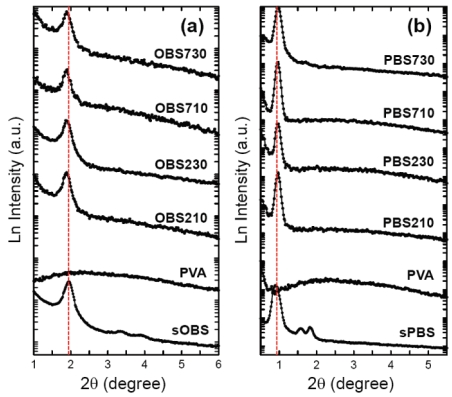

Figure 4. Representative SAXS patterns for two kinds of PVA/sulfonated mesoporous benzene-silica hybrid membranes: (a) for the PVA/SSA/sOBS membrane and (b) for the PVA/SSA/sPBS membrane, respectively. SAXS patterns for PVA matrix and sulfonated mesoporous benzene-silica materials are presented as reference data. Respective sample labels for composite membranes are indicated in (a) and (b).

silica materials is influenced by the nature of the templates used, and the sOBS sample with smaller pores has larger interfacial areas than the sPBS sample with larger pores.

Structural Characterization of PVA/SSA/Mesoporous Benzene-silica Hybrid Composite Membranes. Two series of hybrid membranes were prepared with poly(vinyl alcohol), sulfosuccinic acid, and sulfonated mesoporous benzene-silicas (sOBS and sPBS) as described in the Experimental Section. The compositions of these materials in the final composite membranes are listed in Table 1. Representative small-angle X-ray scattering patterns for the two kinds of composite membranes are shown in Figure 4. As can be seen from Figure 4, all of the composite membranes display a high intense peak, and the corresponding *d*-spacing values are 4.48 and 9.29 nm, respectively, which are the same as those of the sulfonated powders, indicating that the sulfonated mesoporous benzene-silicas inside the PVA/SSA cross-linked polymer matrix maintain uniform mesopores. High-order peaks indicating the presence of an ordered 2D hexagonal mesostructure are not observed in the patterns of the composite membranes but appear partially after repeated measurements using different samples taken from the same membrane. From this result, the following two postulations can be suggested: one is the reduction in the difference of the electron density in the composite membranes through the covering on the mesoporous materials and the penetration into the mesopores of the PVA chains and the SSA molecules, and the other is the distortion of the hexagonally ordered mesostructure through the chemical reaction between the hydroxyl groups in the mesoporous benzene-silica and the carboxylic acid in the SSA molecules, which is similar to the esterification reaction between the PVA chains and the SSA molecules.

The representative WAXS patterns are shown in Figure 5. The blue dotted lines in Figure 5(a-1, a-2, and a-3) represent the semicrystallized region of the PVA polymer chains, and the characteristic length ($2\theta = 19°$, $d = 4.7$ Å) of the crystallized part is maintained in spite of the chemical links with the SSA chains. Figure 5(b,c) corresponds to the two kinds of composite membranes containing the sulfonated mesoporous benzene-silicas of sOBS and sPBS. The WAXS patterns shown in the lowest part of Figure 5(b,c) are for the sOBS and sPBS powder samples, respectively, before mixing them with the PVA matrix polymers. As can be seen in Figure 5(b,c), the intensity of the characteristic peaks for the periodic arrangement of benzene-bridging groups at $2\theta = 11.5$ and 23° (indicated as red dotted

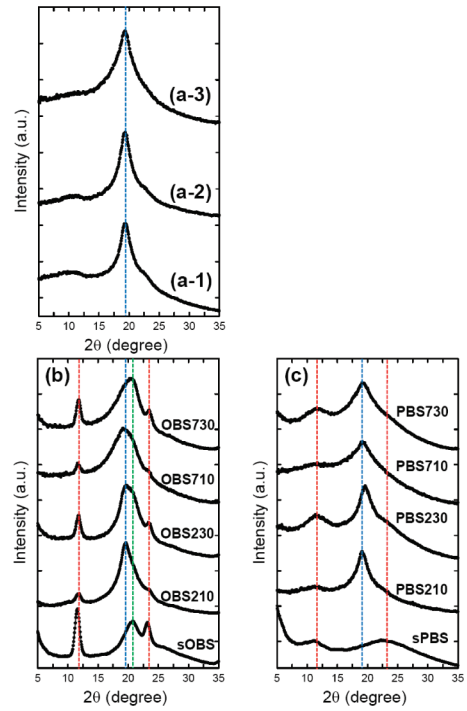

Figure 5. Representative WAXS patterns for PVA and PVA/SSA membranes without mesoporous benzene-silicas (a) and for two kinds of PVA/SSA/sulfonated mesoporous benzene-silica hybrid membranes (b, c): (a-1) is for PVA, (a-2) is for a PPA/SSA membrane containing 2 wt % of SSA, and (a-2) is for a PVA/SSA membrane containing 7 wt % of SSA; (b) is for sOBS and PVA/SSA/sOBS membranes; and (c) is for sPBS and PVA/SSA/sPBS membranes, respectively. Respective sample labels for composite membranes are indicated inside (b) and (c).

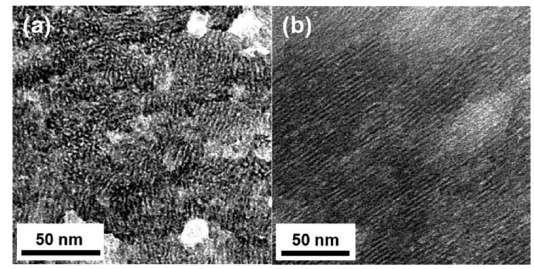

Figure 6. Representative FE-TEM images for the PVA/SSA/sOBS (OBS520) composite membrane: (a) perpendicular and (b) parallel to the cylinder axis.

lines in Figure 5) increases according to the quantity of mesoporous materials inserted (i.e., the peak intensities of the OBS730, OBS230, PBS730, and PBS230 samples are higher than those of the other composite membranes). The characteristic peaks of pure PVA are also maintained in the composite membranes, as shown in Figure 5(b,c). The WAXS results show that the periodic arrangement formed from the benzene-bridging groups and the silica inside the condensed mesoporous walls, as well as the characteristic length scale of the crystallized parts in the PVA chains, are still maintained in spite of the mixing process with the PVA chains and the SSA molecules containing reactive functional groups.

The FE-TEM images of a representative OBS520 composite membrane are shown in Figure 6. Figures 6(a) and 6(b) are taken along different axes, and Figure 6(a) is an enlarged image of the cross section of the OBS520 membrane. These figures clearly show that the composite membrane contains mesoporous benzene-silica materials without loss of the characteristics of

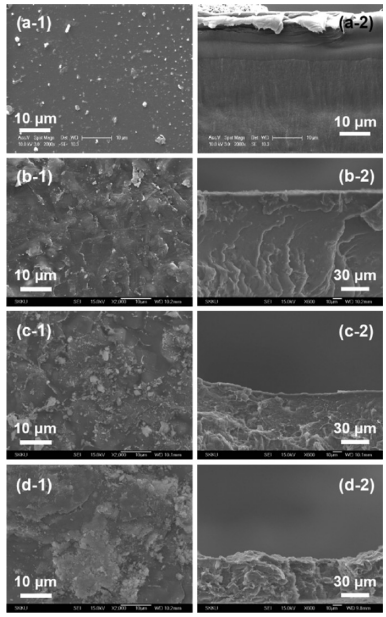

Figure 7. Representative SEM images for the surface and the cross section of PVA/SSA/(sOBS) composite membranes: (a-1) and (a-2) are for PVA/SSA containing 5 wt % of SSA; (b-1) and (b-2) are for the OBS510 membrane; (c-1) and (c-2) are for OBS520; and (d-1) and (d-2) are for OBS530, respectively.

the mesopores. However, Figure 6(a) shows that the 2D hexagonal structured sOBS powder does not maintain its highly ordered mesophases in the mixed membrane, in comparison with the TEM image in Figure 1(a-2), which corresponds to the SAXS results in Figure 4. The TEM image in Figure 6(a), as well as the SAXS pattern in Figure 4, support the conclusion that the esterification reaction between the hydroxyl group in mesoporous benzene-silica and the carboxylic acid in SSA is likely to happen on the inner and outer surfaces of the mesopores in the composite membranes prepared in this study and, consequently, that the ordered hexagonal structure is not maintained.

The SEM images of the PVA/SSA/sOBS composite membranes are shown in Figure 7. The left panels (a-1, b-1, c-1, and d-1) in Figure 7 are the surface images, and the right panels (a-2, b-2, c-2, and d-2) are the cross sectional images for the PVA/SSA membrane containing 5 wt % of SSA and the OBS510, OBS520, and OBS530 composite membranes, respectively. As the content of sulfonated benzene-silica increases up to 30 wt %, the roughness in the surface and cross section also increases.

The SEM-EDS images for the OBS520 composite membrane are shown in Figure 8. Figure 8 shows clearly that the respective atoms for the carbon, oxygen, silicon, and sulfur species are distributed homogeneously inside the PVA/SSA/sOBS composite membrane. The weight percent of sulfur is obtained as 2.5 wt %, which is lower than the value of 3.3 wt % calculated.

The FT-IR spectra for the membranes prepared in this study are shown in Figure 9. Figure 9(a) shows the pattern for the pure PVA polymer, which shows the characteristic bands of sp^3 C−H stretching at 1428 and 2930 cm^{-1}. The peak at 3345 cm^{-1} is from the O−H stretch, and the peak at 1092 cm^{-1} indicates that these hydroxyl groups are from the C−OH groups in the PVA polymer chains. Figure 9(b) shows the characteristic pattern for the OBS mesoporous benzene-silica materials. The peak at 3435 cm^{-1} is from the stretching of the O−H groups located on the surface of the mesoporous materials. The spectra

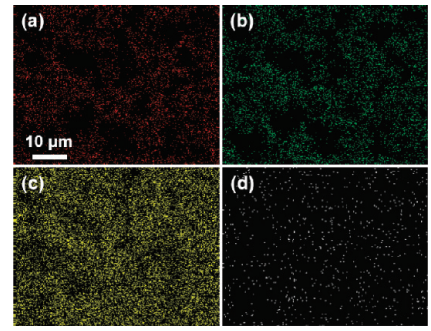

Figure 8. Representative SEM-EDS images for the OBS520 composite membranes: (a) carbon, (b) oxygen, (c) silicon, and (d) sulfur atoms, respectively.

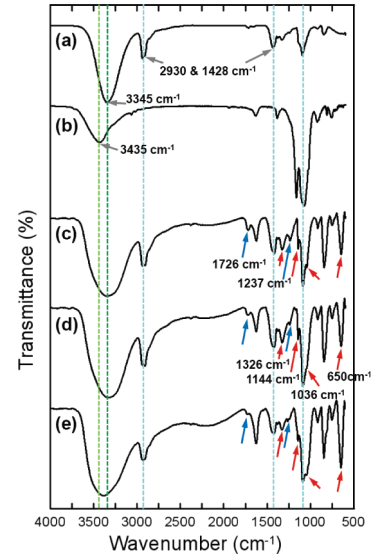

Figure 9. Representative ATR-FTIR spectra for a pure PVA polymer membrane (a), OBS mesoporous material (b), PVA/SSA membrane containing 5 wt % of SSA (c), OBS520 (d), and PBS520 (e) membranes, respectively.

shown in Figure 9(c, d, and e) are for the PVA/SSA membrane containing 5 wt % of SSA cross-linker and for the OBS520 and PBS520 membranes, respectively. The peaks at 650, 1036, 1144, and 1326 cm^{-1} (red arrows in Figure 9) are assigned to S−O and S═O vibrations in the sulfonic acid groups. The S═O vibrations are observed to be separated due to its symmetric-, asymmetric-, and shifted-stretches from two kinds of sulfonic acid groups attached at SSA molecules and benzene-bridging groups, respectively. The peaks at 1237 and 1726 cm^{-1} (blue arrows in Figure 9) are assigned to C−O and C═O vibrations in the ester groups, which are formed from the esterification reaction between the carboxylic acid of SSA and the hydroxyl groups of PVA. Moreover, it would be possible to assign the aforementioned peaks to the other esterification reaction (i.e., ≡Si−O−OC−) between the carboxylic acid of SSA and the hydroxyl groups (≡Si−OH) of mesoporous materials. It is noted that the spectra of all of the membranes indicate the presence of sulfonic acid groups and ester groups, as shown in Figure 9(c, d, and e). In addition, the characteristic peaks (1237 and 1726 cm^{-1}) of the ester groups in Figure 9(e) are the weakest, and those of Figure 9(d) are weaker than those of Figure 9(c), which suggests that the probability of chemical linkages being formed between PVA (or mesoporous materials) and SSA is decreased slightly by the mesoporous materials and that this structural hindrance depends on the morphology of the mesoporous materials. The broad peaks in the range of 3000−3600

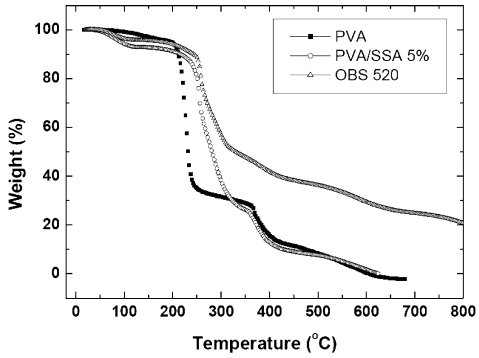

Figure 10. Representative TGA thermograms for pure PVA membrane, PVA/SSA membrane containing 5 wt % of SSA, and OBS520 hybrid composite membrane, respectively.

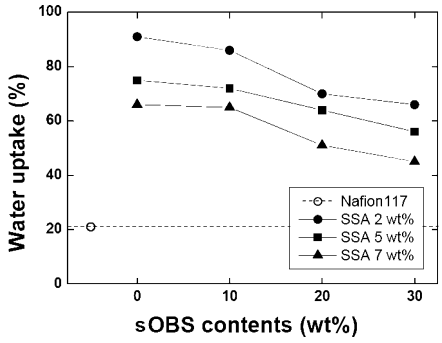

Figure 11. Water uptake for the PVA-based composite membranes according to the contents of SSA and sulfonated mesoporous benzene-silica (sOBS).

cm^{-1} represent the remaining hydroxyl and carboxylic acid groups in the PVA, SSA, and mesoporous materials.

Characterization of PVA/SSA/Mesoporous Benzene-Silica Hybrid Membranes for Fuel Cell Application. The thermal stability of the membranes prepared in this study was investigated using a thermo-gravimetric analyzer under a nitrogen gas flow. As shown in Figure 10, the pure PVA and the composite membranes experience significant weight loss near 200 °C after losing a small quantity (∼5%) of adsorbed water up to 200 °C. The 40−60% weight losses of all the membranes from 200 to 350 °C correspond to the decomposition of the functional groups such as hydroxyl, sulfonic acid, and ester groups. The pure PVA membrane undergoes the degradation step abruptly from 200 °C, while the PVA/SSA and the OBS520 composite membranes are decomposed from 250 °C, which suggests that the cross-linking by the SSA supplement enhances the thermal stability of the membrane. For the OBS520 membrane, the rate of thermal degradation is slower than those of the other membranes, which indicates that the mesoporous benzene-silica materials also enhance the thermal stability of the composite membrane. Figure 10 clearly indicates that the introduction of the mesoporous benzene-silica materials has a positive effect on the thermal stability of the PVA-based hybrid composite membrane in fuel cell applications which are usually operated below 200 °C.

Figure 11 shows the variation of the water uptake for the Nafion117 and the PVA-based composite membranes prepared with the SSA cross-linker and the sulfonated benzene-silica materials (sOBS). As shown in Figure 11, all of the PVA-based membranes exhibit 2.5−4.5 times higher water uptakes than the commercial Nafion117 membrane, which indicates that the hydroxyl groups in the PVA and the sulfonic acid groups in the SSA are very hydrophilic and thus allow a large quantity

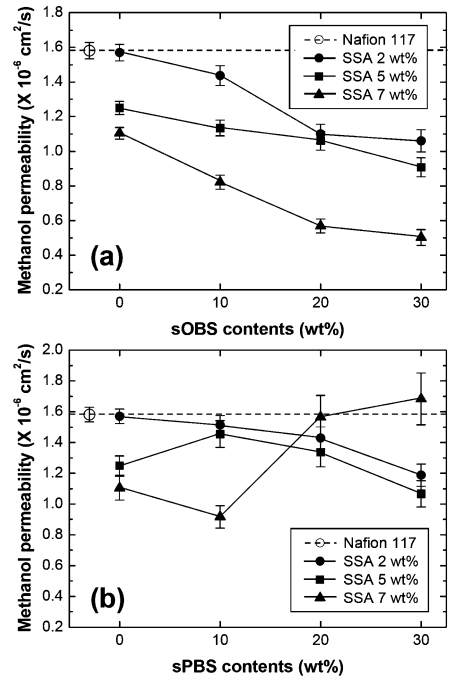

Figure 12. Methanol permeability for the PVA-based composite membranes according to the contents of SSA and sulfonated mesoporous benzene-silicas: (a) PVA/SSA/sOBS and (b) PVA/SSA/sPBS membranes, respectively.

of water to be absorbed. However, the water uptake of the PVA membranes decreases from 95 to 65% as the amount of the SSA cross-linker is increased from 2 to 7%, which is attributed to the reduced free volume in the polymer membranes due to the increased cross-linking density induced by SSA. The water uptake for the series of PVA/SSA/sOBS composite membranes also decreases with increasing contents of the mesoporous materials. This reduction in the water uptake is attributed to the blocking of the water channels and the increased hydrophobicity caused by the addition of the mesoporous benzene-silica materials. However, a high water uptake of over 50% is still maintained even for the OBS730 composite membrane, which is due to the sulfonic acid groups attached on the benzene bridging groups. As a result, the sulfonated mesoporous benzene-silica materials do not have a large negative effect on the water uptake for fuel cell applications, according to the results in Figure 11.

Figure 12 shows the methanol permeability for the Nafion117 and the PVA-based composite membranes prepared with the SSA and the sulfonated benzene-silica materials (sOBS and sPBS). As shown in Figure 12(a), all of the PVA-based membranes exhibit lower methanol permeability than the commercial Nafion117 membrane, and the values decrease as the contents of SSA and sOBS increase up to 7 and 30 wt %, respectively. It is noteworthy that the methanol permeability of the composite membranes containing both sOBS and SSA shows lower values than those of mixed membranes only with an SSA cross-linker depending on the contents of materials used. This result shows clearly that the increased cross-linking density of the PVA polymers afforded by SSA and the blocking of the water channels by the mesoporous benzene-silica (sOBS) are very effective in suppressing the methanol crossover. For example, the methanol permeability of the OBS730 composite membrane is reduced to 5×10^{-7} cm^2/s, whereas that of the pure Nafion117 membrane is 1.58×10^{-6} cm^2/s, which amounts to a 68% reduction in comparison with the Nafion117 membrane. Figure 12(b) shows the methanol permeability for the

PVA/SSA/sPBS composite membranes. In general, the methanol permeability of the sPBS-incorporated PVA membranes shows lower values than that of Nafion117 except for the PBS730 membrane with high contents of sPBS and SSA. However, the sPBS-incorporated PVA membranes show slightly higher values than those of the sOBS-incorporated membranes shown in Figure 12(a), and the composite membranes with high contents (i.e., 5 and 7 wt %) of SSA show an irregular pattern which does not correspond to the contents of sPBS, especially in the case of 7 wt % of SSA. The high methanol permeability shown in Figure 12(b) is attributed to the enhanced diffusivity afforded by the larger pore size of sPBS and the increased size of the water channels brought about by the reduced reaction probability between the PVA polymer chains and SSA cross-linker. The irregular pattern of methanol permeability is attributed to the structural inhomogeneity based on the morphology of sPBS particles. It seems that the chemical reaction between the hydroxyl groups in the PVA polymer chains and the carboxylic acid groups of SSA is likely to be hindered by the large quantity of sPBS particles with a large and rodlike morphology, especially in the case where a large amount of SSA molecules is included in the composite membrane; namely, the cross-linking density between PVA and SSA is reduced when large amounts of sPBS and SSA are mixed with the PVA polymer matrix. Therefore, the size of the water channels in the PVA polymer becomes larger, with some of them being similar in size to those of the pure PVA chains, which explains the high methanol permeability for the PBS720 and PBS730 membranes. The increase in the intensity of the peak at 1624 cm^{-1} in Figure 9(e) also represents the trace of the unreacted carboxylic acid groups in the SSA molecules. Figure 12 indicates clearly that the content of the mesoporous materials as well as SSA has an effect on the methanol permeability. Moreover, the pore size and the morphology of mesoporous materials related with interface in the mixed membrane system are thought to be crucial factors to control the diffusion property of methanol.

The proton conductivity for the composite membranes is shown in Figure 13. As shown in Figure 13(a), the PVA-based membranes containing the sOBS additives exhibit lower proton conductivity than the commercial Nafion117 membrane, except for the PVA/SSA membrane containing 2 wt % of SSA, and the values decrease as the contents of SSA and sOBS increase to 7 and 30 wt %, respectively. Similarly to the lowering of the methanol permeability shown in Figure 12(a), the decreased proton conductivity is attributed to the increased cross-linking density caused by SSA and the blocking of the ion clusters by sOBS. For the OBS730 composite membrane, the proton conductivity is 0.039 S/cm, which corresponds to a 62% reduction compared with that of the Nafion117 membrane of 0.105 S/cm. The proton conductivity data shown in Figure 13(b) are for the series of PVA/SSA/sPBS composite membranes. As can be seen in Figure 13(b), the sPBS-incorporated PVA membranes containing 2 wt % of SSA show the blocking effect of the ion clusters by sPBS to an extent which is dependent on the contents of the materials. However, the sPBS-incorporated PVA membranes containing 5 and 7 wt % of SSA do not show any clear blocking effect, which is attributed to the increased amount of sulfonic acid groups and the reduced cross-linking density of the PVA chains. Figure 13 clearly indicates that the content of mesoporous materials as well as SSA has an effect on the proton conductivity. The pore size and morphology of the mesoporous materials are also very important properties in controlling the proton conductivity effectively.

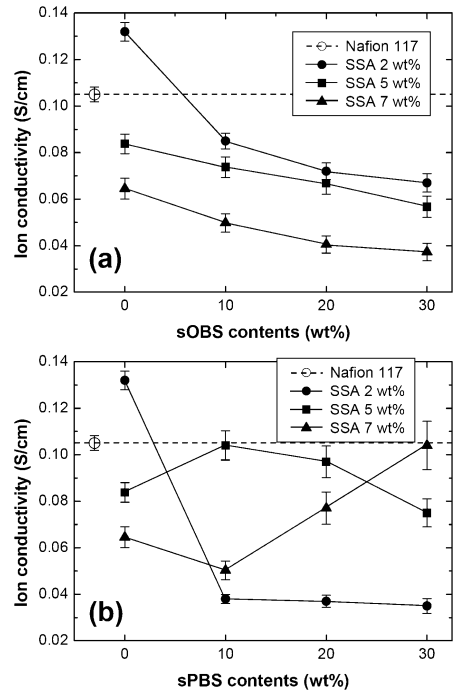

Figure 13. Proton conductivity for the PVA-based composite membranes according to the contents of SSA and sulfonated mesoporous benzene-silicas: (a) PVA/SSA/sOBS and (b) PVA/SSA/sPBS membranes, respectively.

Conclusions

PVA-based composite membranes were prepared with mesoporous benzene-silica materials and a SSA cross-linker, and the nanocomposite membranes were characterized to evaluate the applicability of mesoporous benzene-silica materials as a diffusion controller for DMFC applications. In addition, two kinds of sulfonated mesoporous benzene-silica materials with a 2D hexagonal lattice were prepared using an ODTMA cationic surfactant and a P123 nonionic polymer, to investigate the effect of the pore size and morphology of the mesoporous benzene-silica materials. The structural characterization of the two kinds of sulfonated mesoporous benzene-silica materials was performed using SAXS, TEM, SEM, and nitrogen adsorption analysis. A series of PVA-based hybrid composite membranes containing various amounts of mesoporous benzene-silica and SSA were prepared. The chemical structures of the composite membranes were analyzed by SAXS, WAXS, TEM, SEM, and FT-IR. Also, the thermal stability, water uptake, methanol permeability, and proton conductivity of the composite membranes were investigated for fuel cell membrane applications.

This work clearly demonstrated that the contents of the mesoporous benzene-silica materials as well as the SSA cross-linker have a positive effect on the reduction of the methanol permeability in the preparation of PVA-based composite membranes. Moreover, it is suggested that the morphology and the pore size of mesoporous benzene-silica materials related with interface in the mixed membrane system are crucial factors to control the transport property of methanol and the proton conductivity.

Acknowledgment. This work was supported by the Korea research Foundation Grant (KRF 2006-005-J04601) and by the Korean Science and Engineering Foundation (KOSEF) grant funded by the Korea government (MEST) (No. R0A-2007-000-10029-0) in part. Experiments at PLS were supported in part by MEST and POSTECH.

Supporting Information Available: Three figures showing methanol permeation and proton conductivity, the mechanical properties, and nitrogen adsorption−desorption analysis for the PVA-based nanocomposite membranes. This material is available free of charge via the Internet at http://pubs.acs.org.

References and Notes

(1) Service, R. F. *Science* **2002**, *296*, 1222–1224.
(2) Dillon, R.; Srinvasan, S.; Aricom, A. S.; Antonucci, V. *J. Power Sources* **2004**, *127*, 112–126.
(3) Neburchilov, V.; Martin, J.; Wang, H. J.; Zhang, J. J. *J. Power Sources* **2007**, *169*, 221–238.
(4) Pu, C.; Huang, W.; Ley, K. L.; Smotkin, E. S. *J. Electrochem. Soc.* **1995**, *142*, L119−L120.
(5) Burstein, G. T.; Barnett, C. J.; Kucernak, A. R.; Williams, K. R. *Catal. Today* **1997**, *38*, 425–437.
(6) Heinzel, A.; Barragan, V. M. *J. Power Sources* **1999**, *84*, 70–74.
(7) Inaba, M.; Kinumoto, T.; Kiriake, M.; Umebayashi, R.; Tasaka, A.; Ogumi, Z. *Electrochim. Acta* **2006**, *51*, 5746–5753.
(8) Kinumoto, T.; Inaba, M.; Nakayama, Y.; Ogata, K.; Umebayashi, R.; Tasaka, A.; Iriyama, Y.; Abe, T.; Ogumi, Z. *J. Power Sources* **2006**, *158*, 1222–1228.
(9) Sahu, A. K.; Selvarani, G.; Pitchunami, S.; Sridhar, P.; Shukla, A. K.; Narayanan, N.; Banerjee, A.; Chandrakumar, N. *J. Electrochem. Soc.* **2008**, *155*, B686–B695.
(10) Teranishi, K.; Kawata, K.; Tsushima, S.; Hirai, S. *Electrochem. Solid State Lett.* **2006**, *9*, A475−A477.
(11) Arico, A. S.; Srinivasan, S.; Antonucci, V. *Fuel Cells* **2001**, *1*, 133–161.
(12) Deluca, N. W.; Elabd, Y. A. *J. Polym. Sci., Part B: Polym. Phys.* **2006**, *44*, 2201–2225.
(13) Jagur-Grodzinski, J. *Polym. Adv. Technol.* **2007**, *18*, 785–799.
(14) Yin, Y.; Fang, J. H.; Cui, Y. F.; Tanaka, K.; Kita, H.; Okamoto, K. *Polymer* **2003**, *44*, 4509–4518.
(15) Einsla, B. R.; Kim, Y. S.; Hickner, M. A.; Hong, Y. T.; Hill, M. L.; Pivovar, B. S.; McGrath, J. E. *J. Membr. Sci.* **2005**, *255*, 141–148.
(16) Okamoto, K.; Yin, Y.; Yamada, O.; Islam, M. N.; Honda, T.; Mishima, T.; Suto, Y.; Tanaka, K.; Kita, H. *J. Membr. Sci.* **2005**, *258*, 115–122.
(17) Zhai, F. X.; Guo, X. X.; Fang, J. H.; Xu, H. J. *J. Membr. Sci.* **2007**, *296*, 102–109.
(18) Lee, C. H.; Wang, Y. Z. *J. Polym. Sci., Part A: Polym. Chem.* **2008**, *46*, 2262–2276.
(19) Li, L.; Zhang, J.; Wang, Y. X. *J. Membr. Sci.* **2003**, *226*, 159–167.
(20) Tripathi, B. P.; Shahi, V. K. *J. Colloid Interface Sci.* **2007**, *316*, 612–621.
(21) Yoon, S. R.; Hwang, G. H.; Cho, W. I.; Oh, I. H.; Hong, S. A.; Ha, H. Y. *J. Power Sources* **2002**, *106*, 215–223.
(22) Jung, D. H.; Cho, S. Y.; Peck, D. H.; Shin, D. R; Kim, J. S. *J. Power Sources* **2003**, *118*, 205–211.
(23) Tricoli, V.; Nannetti, F. *Electrochim. Acta* **2003**, *48*, 2625–2633.
(24) Rhee, C. H.; Kim, H. K.; Chang, H.; Lee, J. S. *Chem. Mater.* **2005**, *17*, 1691–1697.
(25) Thomassin, J. M.; Pagnoulle, C.; Caldarella, G.; Germain, A.; Jerome, R. *Polymer* **2005**, *46*, 11389–11395.
(26) Chen, Z. W.; Holmberg, B.; Li, W. Z.; Wang, X.; Deng, W. Q.; Munoz, R.; Yan, Y. S. *Chem. Mater.* **2006**, *18*, 5669–5675.
(27) Thomassin, J. M.; Pagnoulle, C.; Bizzari, D.; Caldarella, G.; Germain, A.; Jerome, R. *Polymer* **2006**, *177*, 1137–1144.
(28) Lin, Y. F.; Yen, C. Y.; Ma, C. C. M.; Liao, S. H.; Hung, C. H.; Hsiao, Y. H. *J. Power Sources* **2007**, *165*, 692–700.
(29) Lin, Y. F.; Yen, C. Y.; Hung, C. H.; Hsiao, Y. H.; Ma, C. C. M. *J. Power Sources* **2007**, *168*, 162–166.
(30) Chiang, W. Y.; Hu, C. M. *J. Appl. Polym. Sci.* **1991**, *43*, 2005–2012.
(31) Rhim, J. W.; Yeom, C. K.; Kim, S. W. *J. Appl. Polym. Sci.* **1998**, *68*, 1717–1723.
(32) Pivovar, B. S.; Wang, Y. X.; Cussler, E. L. *J. Membr. Sci.* **1999**, *154*, 155–162.
(33) Rhim, J. W.; Park, H. B.; Lee, C. S.; Jun, J. H.; Kim, D. S.; Lee, Y. M. *J. Membr. Sci.* **2004**, *238*, 143–151.
(34) Kim, D. S.; Park, H. B.; Rhim, J. W.; Lee, Y. M. *J. Membr. Sci.* **2004**, *240*, 37–48.
(35) Qiao, J.; Hamaya, T.; Okada, T. *J. Mater. Chem.* **2005**, *15*, 4414–4423.
(36) Hamaya, T.; Inoue, S.; Qiao, J.; Okada, T. *J. Power Sources* **2006**, *156*, 311–314.
(37) Yang, C.-C.; Chiu, S.-J.; Chien, W.-C. *J. Power Sources* **2006**, *162*, 21–29.
(38) DeLuca, N. W.; Elabd, Y. A. *J. Membr. Sci.* **2006**, *282*, 217–224.
(39) Sairam, M.; Naidu, B. V. K.; Nataraj, S. K.; Sreedhar, B.; Aminabhavi, T. M. *J. Membr. Sci.* **2006**, *283*, 65–73.
(40) Jia, X.; Li, Y.; Cheng, Q.; Zhang, S.; Zhang, B. *Eur. Polym. J.* **2007**, *43*, 1123–1131.
(41) Kresge, C. T.; Leonowicz, M. E.; Roth, W. J.; Vartuli, J. C.; Beck, J. S. *Nature* **1992**, *359*, 710–712.
(42) Yang, H.; Coombs, N.; Ozin, G. A. *Nature* **1997**, *386*, 692–695.
(43) Zhao, D.; Feng, J.; Huo, Q.; Melosh, N.; Fredrickson, G. H.; Chmelka, B. F.; Stucky, G. D. *Science* **1998**, *279*, 548–552.
(44) Ying, J. Y.; Mehnert, C. P.; Wong, M. S. *Angew. Chem., Int. Ed.* **1999**, *38*, 56–77.
(45) Sanchez, C.; Soler-Illia, G. J. de A. A.; Ribbot, F.; Lalot, T.; Mayer, C. R.; Cabuil, V. *Chem. Mater.* **2001**, *13*, 3061–3083.
(46) Inagaki, S.; Guan, S.; Fukushima, Y.; Ohsuna, T.; Terasaki, O. *J. Am. Chem. Soc.* **1999**, *121*, 9611–9614.
(47) Melde, B. J.; Holland, B. T.; Blandford, C. F.; Stein, A. *Chem. Mater.* **1999**, *11*, 3302–3308.
(48) Asefa, T.; MacLachlan, M. J.; Coombos, N.; Ozin, G. A. *Nature* **1999**, *402*, 867–871.
(49) Goto, Y.; Inagaki, S. *Chem. Commun.* **2002**, 2410–2411.
(50) Inagaki, S.; Guan, S.; Ohsuna, T.; Terasaki, O. *Nature* **2002**, *416*, 304–307.

JP9006763